

Multi-phase rotational angiography of the left ventricle to assist ablations: feasibility and accuracy of novel imaging.

Jean-Yves Wielandts, MD, MSc^{1,2}, Stijn De Buck, MSc, PhD^{2,3}, Koen Michielsen, MSc^{2,4}, Ruan Louw, MD¹, Christophe Garweg, MD¹, Johan Nuyts, MSc, PhD^{2,4}, Joris Ector, MD, PhD¹, Frederik Maes, MSc, PhD^{2,3,5}, Hein Heidbuchel, MD, PhD⁶

¹Department of Cardiovascular Sciences, KU Leuven, Belgium

²Medical Imaging Research Centre, KU Leuven & UZ Leuven, Belgium

³Department of Electrical Engineering, ESAT/PSI, Medical Image Computing, KU Leuven, Belgium

⁴Department of Nuclear Medicine and Molecular Imaging, KU Leuven, Belgium

⁵iMinds-Future Health Department, KU Leuven, Belgium

⁶Hasselt University and Heart Center Hasselt, Belgium

Short Title: Multi-Phase 3DRA of LV: feasibility and accuracy

Address for correspondence:

Jean-Yves Wielandts, MD, MSc.

Cardiology - Medical Imaging Research Centre

University Hospital Gasthuisberg

Herestraat 49

B-3000 Leuven, Belgium

Phone: +32 16341554

Fax: +32 16344240

Email: jean-yves.wielandts@uzleuven.be

Word count: 4973 words

Funding and potential conflicts of interest.

J-Y.W. and J.E. are supported by a grant of the Research Foundation Flanders. H.H. is holder of the AstraZeneca Chair in Cardiac Electrophysiology, University of Leuven. H.H. and S.D.B received research funding through the University of Leuven from Siemens Medical Solutions. H.H. is Coordinating Clinical Investigator for the Biotronik-sponsored EuroEco study on health-economics of remote device monitoring. H.H. is a member of the scientific advisory board of General Electric, Siemens Medical Solutions, Boehringer-Ingelheim, Bayer, Daiichi-Sankyo, BMS/Pfizer and Sanofi-Aventis, and receives unconditional research grants through the University of Leuven from St Jude Medical, Medtronic, Biotronik and Boston Scientific Inc.. S.D.B. is supported by an IWT grant for unrelated research.

Abstract:

Aims: Interventional LV procedures integrating static 3D anatomy visualisation are subject to mismatch with dynamic catheter movements due to prominent LV motion. We aimed to evaluate the accuracy of a recently developed acquisition and post-processing protocol for low radiation dose LV multi-phase Rotational Angiography (4DRA) in patients.

Methods and Results: 4DRA image acquisition of the LV was performed as investigational acquisition in patients undergoing left sided ablation (11 men; BMI=24.7±2.5kg/m²). Iodine contrast was injected in the LA while pacing from the RA at a cycle length of 700ms. 4DRA acquisition and reconstruction was possible in all 11 studies. Reconstructed images were post-processed using streak artefact reduction algorithms and an inter-phase registration-based filtering method, increasing contrast-to-noise-ratio by a factor 8.2±2.1. This enabled semi-automatic segmentation, yielding LV models of 5 equidistant phases per cardiac cycle. For evaluation, off-line 4DRA-fluoroscopy registration was performed and the 4DRA LV contours of the different phases were compared to the contours of 5 corresponding phases of biplane LV angiography, acquired in identical circumstances. Of the distances between these contours, 95% were <4mm in both incidences. Effective radiation dose for 4DRA, calculated by patient-specific Monte-Carlo simulation, was 5.1±1.1mSv.

Conclusions: Creation of 4DRA LV models in man is feasible at near-physiological heart rate and with clinically acceptable radiation dose. They showed high accuracy with respect to LV angiography in RAO and LAO. The presented technology not only opens perspectives for full cardiac cycle dynamic anatomical guidance during interventional procedures, but also for 3DRA without need for very rapid pacing.

Key Words: angiography, catheter ablation, imaging, tomography, ventricle

Introduction.

Integrating highly detailed visualisation of relevant anatomical structures during complex ablation procedures results in net clinical benefit: fusion of three dimensional models in electro-anatomical mapping (EAM) systems or fluoroscopy-based systems has been reported to be beneficial for safety, accuracy, total radiation exposure, procedural duration and/or clinical outcomes.¹⁻⁸

Recently, rotational angiography (3DRA) has been put into use to generate 3D tomographic reconstructions of contrast-filled cardiac cavities. To optimise accuracy, acquisition needs to be performed during virtual cardiac standstill, i.e. by using adenosine or fast ventricular pacing at rates $\geq 200/\text{min}$, which may induce atrial and ventricular arrhythmias and cannot be performed in an awake patient. The 3DRA techniques match pre-procedural CT and MRI for accurate imaging of anatomical structures relevant to the ablation procedure.⁹⁻¹³ Moreover, 3DRA compares favourably to even state-of-the art and prospectively ECG-gated CT in terms of iodine contrast administration and patient radiation dose.¹³⁻¹⁹ Its integration with EAM systems is feasible and stand-alone registration of 3DRA generated models to fluoroscopy has also been shown to be an effective strategy.^{13,18-21} Also because of its logistical advantages and superiority for intermodal registration, it is becoming the modality of choice for intra-procedural 3D imaging.

To date, the predominant part of clinical studies evaluated 3DRA in the setting of atrial fibrillation ablation. For that purpose, static 3D models of the left atrium (LA) and pulmonary veins seem to suffice due to limited relative movement of the structures of interest for ablation throughout the cardiac cycle.^{22,23} However, when the region of interest is subject to more prominent cardiac motion, particularly in the case of left ventricular (LV) ventricular tachycardia (VT) ablations, feedback of real time relative catheter position, by means of fluoroscopy or catheter-tracking EAM systems, will inherently be of high cyclic inaccuracy when projected on a static 3D model.

Initial studies have recently shown the feasibility of generating multi-phase 3D (i.e. 4D) rotational angiography models, although often at the cost of unacceptably high radiation dose. Moreover, validation of their accuracy for real-time heart motion in clinical context is still lacking.²⁴⁻²⁸

In this study we aimed to assess feasibility, accuracy and validity of a novel low-radiation acquisition and post-processing protocol for generating highly detailed 4D models of the LV at a near-physiological heart rate.

Methods.

3DRA Acquisition

Multi-phase 3DRA was performed in 11 consecutive patients (11 men; aged 56±16 years) referred for left-sided ablation: PVI (n=7), post-ischaemic VT (n=1), LVOT (n=2) and left lateral accessory pathway (n=1), using a Siemens Axiom Artis System. The acquisition was performed as an investigational protocol for off-line analysis, i.e. not for use during the procedure itself. This was required by the local ethics committee as it was the first study in man. Informed consent was obtained from all patients. Patients with iodine allergy or increased risk for contrast-induced nephropathy were excluded from this study (age>75 years, CrCl<60 ml/min, diabetes, anaemia and/or proteinuria).²⁹

Patient height, weight and BMI were 178±10 cm, 78±9 kg and 24.7±2.5 kg/m², respectively.

Iodine contrast agent (low-osmolar, 37.2±2.2 g-I, 94.9±3.5 ml) was administered, during right atrial (RA) pacing at a cycle length of 700 ms, through a transseptal pigtail catheter in the LA while 100 projections were acquired in a single 14 sec 200° C-arm rotation around the patient during apnoea and using optimal radiation field collimation (73.5±7.8 % of detector height). The protocol imaged 5 equidistant cardiac phases with 20 projections each. Effective radiation dose was calculated in a patient-specific way by means of a Monte-Carlo simulation-based method, using the frame-specific relevant DICOM data (mAs, kVp and incidence of radiation) and the most recent ICRP definition.^{30,31}

Reconstruction, Segmentation and Image Integration

In order to prevent streak artifacts originating from high density materials at reconstruction (e.g. catheter tips, oesophageal probes, external metal on the body surface, etc...), a projection completion method was applied.³² In brief, this algorithm uses an initial 3D image reconstruction based on all 100 projections (i.e. irrespective of cardiac phase), from which all high density materials

are segmented by means of gray value thresholding. These segmented regions are then projected using the system geometry to find their corresponding areas in the original projection data, which are replaced by a linear interpolation of surrounding densities. The updated projections were subsequently used to reconstruct each of the 5 phases separately (i.e. using 20 projections), effectively replacing high-density structures by a local interpolation of surrounding densities. All reconstructions were performed on an off-line dedicated Siemens 3D workstation with a 0.925 mm voxel resolution.

The reconstructed 3D images were post-processed for noise and residual artefact reduction using an inter-phase registration-based (IPR) filtering method, adapted from *Wielandts et al.*,²⁴ to increase contrast-to-noise-ratio (CNR) and enable semi-automatic LV cavity segmentation. This method implicitly defines a mathematical relation between the voxels in the 3D images of all 5 phases so that segmentation of a single phase is sufficient to generate the segmentations of the 4 remaining phases. Semi-automatic segmentation of the phase closest to mid-diastole was performed using an in-house developed tool (*EPSegmenter*, previously reported in *De Buck et al.*¹⁵).²⁴

In all patients, LV angiography sequences were acquired at 15 frames per second, using the Axiom Artis biplane fluoroscopy system ($37.7 \pm 7.5^\circ$ RAO, $52.7 \pm 7.2^\circ$ LAO), during identical pacing conditions and by administering iodine contrast agent (low-osmolar, 21 ± 0 g-I, 60 ± 0 ml) through the transseptal pigtail catheter in the LA. Retrospectively, 5 angiogram frames were selected based on DICOM ECG information to match the 5 acquired 3DRA phases.

Image integration of the 5-phase 4D model with the fluoroscopy system was achieved in RAO and LAO by means of landmark-based registration using an in-house developed software for electro-anatomical mapping (*LARCA*, as described in *Ector et al.*¹). All 5 acquired phases were used to define the optimal 4D-fluoroscopy registration parameters.

Quality Assessment

Comparing the originally reconstructed images and the post-processed images was done using CNR as objective index of image quality. CNR was defined as the difference between cavity signal intensity and wall signal intensity, divided by image noise. Signal intensity was defined as the mean gray value inside 3 large regions of interest (ROI) for the LV cavity (at basal, mid and apical level) and 7 ROIs for the LV wall (apical, baso- and mid-septal, baso- and mid-lateral, anterior and posterior region). Identical ROIs were used in the corresponding images before and after image post-processing. Image noise was derived from averaged standard deviations of the gray values in the same ROIs. Similarly, CNR was calculated on static 3DRA reconstructions made for guidance of VT ablations in a comparable retrospectively selected population (11 men, aged 53 ± 14 years, BMI 25.8 ± 5.3 kg/m 2), using a clinical acquisition protocol as described in *De Buck et al.*¹⁵ In a single 4 sec 200° C-arm rotation around the patient, 67 projection images are acquired during apnoea and joint rapid A-V pacing at a cycle length of 250 ms, after iodine contrast agent (low-osmolar, 15.8 ± 0 g-I) administration in the left ventricle.

In order to assess 4D model accuracy, the 5 phase models were projected in RAO and LAO using the registration parameters defined in the image integration step and their contours were automatically extracted using a Sobel edge detection filter. The LV cavity was manually delineated in the corresponding angiography frames and similarity to the 4D model projections was evaluated using the closest point distance and the Dice coefficient as measure of spatial overlap.³³

Statistical Analysis

All data was analyzed using IBM SPSS. Descriptive data for continuous variables are presented as mean \pm sd. Normality was checked by the Shapiro-Wilk test. Normally distributed data were compared with normal-model based analysis of variance. The level of significance was set at 0.05.

Results.

Image Quality

Figure 1 illustrates image quality improvement after streak artefact reduction and inter-phase registration-based filtering for a mid-systolic phase in one patient. The quantitative data for the reconstructed images before and after post-processing are shown for all 5 phases and all experiments in *Table 1*. While signal intensity in both LV cavity and LV wall remained approximately unchanged, an 86.3% decrease in noise was noted, increasing contrast-to-noise ratio (CNR) to 5.7 ± 1.9 .

Corresponding quantitative data for the clinical static 3DRA reconstructions, which can be segmented accurately without additional post-processing, are reported in Table 1.¹⁵ Their CNR was 3.8 ± 1.0 , due to a three times higher cavity-wall contrast and 44.3% less noise than unprocessed 4DRA reconstructions.

4D Model Accuracy

Examples of segmentations of a diastolic (blue) and systolic (green) phase in the same patient are shown in *Figure 2* and the respective overlays with their corresponding angiography frames in RAO and LAO in *Figure 3*. This is also shown in a video that can be downloaded from the online supplement. Similarity evaluation between the projected contours of the 4D models and the delineation of the corresponding angiography frames yielded the results as summarised in *Table 2*. There was no significant difference in similarity measures with respect to viewing angle or stage in the cardiac cycle, except for the Dice overlap measure, which was significantly higher in LAO than in RAO.

Radiation Dose

Monte-Carlo simulations yielded an average approximate effective radiation dose for 4DRA of 5.1 ± 1.1 mSv. This corresponded to a peri-procedurally available DAP-value of 24.3 ± 4.9 Gy cm². The relation between system-reported DAP, available during the procedure, and calculated effective dose

(ED) is shown in *Figure 4*. Linear regression ($R^2=0.73$) yields $ED = m*DAP$, with the conversion factor $m = 0.21 \text{ mSv/Gycm}^2$, corresponding to previously published values.¹⁴

Timing Implications

A detailed description of the ± 13 min time needed to generate a 5-phase 4DRA segmentation is shown in *Figure 5* and put in contrast to the ± 4 min needed for a single-phase 3DRA segmentation, as described in *Wielandts et al.*²⁴ Following the acquisition, an initial reconstruction based on all 100 acquired projection images is performed in ± 1 min, before application of the streak artifact reduction method, requiring ± 3.5 min. The separate reconstruction of the 5 phases based on the updated projection images and the application of the IPR-based filtering method each take ± 2 min. The segmentation step requires ± 3.5 min.

Discussion

Three dimensional rotational angiographic image integration, for combining highly detailed anatomical information with dynamic catheter tracking, has shown its added value in complex ablation procedures. Its clinical use has however been limited to static 3D imaging of the chamber of interest, which entails important cyclic mismatch for locations subject to prominent cardiac motion, like the ventricles. The acquisition and post-processing protocols evaluated in this study show the ability to create highly accurate 4DRA LV models in man at near-physiological heart rate and with low radiation dose. Currently, dynamic 3D surface anatomy reconstruction is not available in commercial electro-anatomical mapping systems with or without intracardiac echography integration, while 4D trans-thoracic and trans-esophageal echography have considerable practical limitations for LV imaging during ablation procedures. Feasibility of 4D intracardiac echography has recently been shown in initial prototype studies, but clinical use remains impeded by technical difficulties related to catheter mechanics and image quality.³⁴⁻³⁶

High radiation dose has so far been the main restriction for applying dynamic radiographic imaging since the available protocols required the acquisition of a large amount of projection data to allow

reconstruction and segmentation. In contrast, the presented method limits radiation exposure by using sparse projection data to reconstruct each phase, which results in more prominent image noise and artefacts. These are circumvented by streak artefact reduction methods and by integrating image information from all phases using an interphase registration approach.²⁴ Notwithstanding a three times lower cavity-to-wall contrast than in typical static 3DRA images, the resulting noise reduction, amounting to 86.3%, and increase of the contrast-to-noise ratio, by a factor 8.2, enables quick semi-automatic segmentation. This way, 100 projections suffice to obtain segmentations of 5 distinct cardiac phases, at an acceptable estimated effective dose of 5.1 mSv compared to static (i.e. single phase) 3D imaging using 3DRA (2.6 mSv) or state-of-the-art prospective gated CT (1.9 mSv) and at a very acceptable estimated effective dose compared to retrospective gated CT, which enables multi-phase reconstruction (23.2 mSv).^{14-16,37}

Importantly, our approach uses near-physiological atrial pacing at a rate of 85 bpm, which provides a controlled rate above the intrinsic rate that allows perfect synchronisation of C-arm imaging with the cardiac cycle. Unlike static 3D imaging using rapid ventricular pacing (at rates above 220 bpm) or administration of high doses of adenosine,^{10,18} this approach does not necessitate sedation or general anaesthesia, avoids the risk of inducing ventricular fibrillation, and respects the natural dynamics of ventricular contraction.

Finally, an acceptable iodine contrast load was used despite the fact that, unlike in static 3D imaging, the blood-contrast pool is not constrained to the chamber of interest due to preserved cardiac contraction and continuous contrast infusion is required to maintain opacification. The amount of iodine contrast still enables application in patients with reduced kidney function, even when applying a strict cut-off (i.e. CrCl<60 ml/min and/or proteinuria) in the prevention of contrast-induced nephropathy.²⁹ In this study, the amount of contrast was independent of patient weight, but we postulate that this can likely be reduced in slender patients.

Our validation data show that when the 4D LV model is compared with angiographic controls in conventional RAO and LAO fluoroscopy, high anatomical accuracy is obtained independent of

viewing angle and stage in the cardiac cycle. The trend towards better similarity in LAO compared to RAO is explained by the more limited variation in LV cavity cross section throughout the cardiac cycle in LAO view. Around 95% of distances between the 4D and angiographic contours were inferior to 4 mm in both incidences. We considered 4 mm a valid application-specific cut-off value for tolerable errors, since ventricular ablation lesions, which are usually deployed with irrigated catheters, easily reach a width of 4mm.³⁸

The presented technology not only opens perspectives for full cardiac cycle dynamic anatomical guidance during interventional procedures. It also allows multi-phase 3DRA in awake patients, without need for virtual cardiac standstill and thus imaging of physiologic contractile states, for use in current EAM systems or fluoroscopy-based approaches.

This study has some limitations. Since this was an off-line evaluation, clinical prospective evaluation should include impact on ablation outcome and process indicators, like total procedural radiation dose and duration, to define where the use of the presented protocol might prove beneficial. Due to very strict a-priori exclusion criteria, only male patients could be included in this study. Although there are no technical limitations to apply the method to female subjects, they tend to have higher effective radiation doses due to a higher relative radiation risk. For radiographic examinations of the thoracic region, this relative risk increase can be estimated at 1.33 in adult women compared to adult men.^{14,39} We used atrial pacing only, to preserve normal AV conduction and ventricular contraction. It needs to be evaluated to what extent ventricular pacing in patients in whom atrial pacing cannot be used results in clinically useful 4D images of the LV. A priori selection of specific cardiac phases is not yet possible due to technical constraints in current rotational imaging systems. The results of this feasibility study may spur adaptation of existing systems in the future. More efficient method implementation into the reconstruction workstation will reduce post-processing complexity and duration. Iterative reconstruction methods could further reduce noise and streak artifacts, but their implementation requires intermediary image data which is not available from

commercial acquisition systems and hence the impact of such additional technology could not be evaluated in this study.^{27,28,40,41}

Conclusions

We have shown that creation of 4DRA LV models in man is feasible at near-physiological heart rate and with clinically acceptable radiation dose and iodine contrast administration. In this exploratory study, the models accurately reflect the dynamic deformation of the LV throughout the cardiac cycle as validated with respect to LV angiographic images in RAO and LAO. The presented technology not only opens perspectives for full cardiac cycle dynamic anatomical guidance during interventional procedures using dynamic catheter tracking, but also for 3DRA in fully awake patients, without the need for virtual cardiac standstill, thereby avoiding the risk of inducing unwanted ventricular arrhythmias.

References.

1. Ector J, De Buck S, Huybrechts W, Nuyens D, Dymarkowski S, Bogaert J, *et al.* Biplane three-dimensional augmented fluoroscopy as single navigation tool for ablation of atrial fibrillation: accuracy and clinical value. *Heart Rhythm* 2008; **5**: 957-64.
2. Martinek M, Nesser HJ, Aichinger J, Boehm G, Purerfellner H. Impact of integration of multislice computed tomography imaging into three-dimensional electroanatomic mapping on clinical outcomes, safety, and efficacy using radiofrequency ablation for atrial fibrillation. *Pacing Clin Electrophysiol* 2007; **30**: 1215-23.
3. Bertaglia E, Bella PD, Tondo C, Proclemer A, Bottini N, De Ponti R, *et al.* Image integration increases efficacy of paroxysmal atrial fibrillation catheter ablation: results from the CartoMerge Italian Registry. *Europace* 2009; **11**: 1004-10.
4. Caponi D, Corleto A, Scaglione M, Blandino A, Biasco L, Cristoforetti Y, *et al.* Ablation of atrial fibrillation: does the addition of three-dimensional magnetic resonance imaging of the left atrium to electroanatomic mapping improve the clinical outcome? : a randomized comparison of Carto-Merge vs. Carto-XP three-dimensional mapping ablation in patients with paroxysmal and persistent atrial fibrillation. *Europace* 2010; **12**: 1098-104.
5. Della Bella P, Fassini G, Cireddu M, Riva S, Carbucicchio C, Giraldi F, *et al.* Image integration-guided catheter ablation of atrial fibrillation: a prospective randomized study. *J Cardiovasc Electrophysiol* 2009; **20**: 258-65.
6. Tops LF, Schalij MJ. Multislice CT: is it essential before atrial fibrillation ablation? *Heart* 2008; **94**: 973-5.
7. Dong J, Calkins H, Solomon SB, Lai S, Dalal D, Lardo AC, *et al.* Integrated electroanatomic mapping with three-dimensional computed tomographic images for real-time guided ablations. *Circulation* 2006; **113**: 186-94.

8. Sommer P, Rolf S, Piorkowski C, Gaspar T, Huo Y, Piedra C, *et al.* Nonfluoroscopic Catheter Visualization in AF Ablation: Experience from 375 Consecutive Procedures. *Circ Arrhythm Electrophysiol* 2014; **7**: 869-74.
9. Thiagalingam A, Manzke R, D'Avila A, Ho I, Locke AH, Ruskin JN, *et al.* Intraprocedural volume imaging of the left atrium and pulmonary veins with rotational X-ray angiography: implications for catheter ablation of atrial fibrillation. *J Cardiovasc Electrophysiol* 2008; **19**: 293-300.
10. Ector J, De Buck S, Nuyens D, Rossenbacker T, Huybrechts W, Gopal R, *et al.* Adenosine-induced ventricular asystole or rapid ventricular pacing to enhance three-dimensional rotational imaging during cardiac ablation procedures. *Europace* 2009; **11**: 751-62.
11. Nölker G, Gutleben KJ, Marschang H, Ritscher G, Asbach S, Marrouche N, *et al.* Three-dimensional left atrial and esophagus reconstruction using cardiac C-arm computed tomography with image integration into fluoroscopic views for ablation of atrial fibrillation: accuracy of a novel modality in comparison with multislice computed tomography. *Heart Rhythm* 2008; **5**: 1651-7.
12. Kriatselis C, Nedios S, Akrivakis S, Tang M, Roser M, Gerds-Li JH, *et al.* Intraprocedural imaging of left atrium and pulmonary veins: a comparison study between rotational angiography and cardiac computed tomography. *Pacing Clin Electrophysiol* 2011; **34**: 315-22.
13. Li JH, Haim M, Movassagh B, Mendel JB, Chaudhry GM, Haffajee CI, *et al.* Segmentation and registration of three-dimensional rotational angiogram on live fluoroscopy to guide atrial fibrillation ablation: a new online imaging tool. *Heart Rhythm* 2009; **6**: 231-7.
14. Heidbuchel H, Wittkampf FH, Vano E, Ernst S, Schilling R, Picano E, *et al.* Practical ways to reduce radiation dose for patients and staff during device implantations and electrophysiological procedures. *Europace* 2014; **16**: 946-64.

15. De Buck S, Alzand BS, Wielandts JY, Garweg C, Phlips T, Ector J, *et al.* Cardiac three-dimensional rotational angiography can be performed with low radiation dose while preserving image quality. *Europace* 2013; **15**: 1718-24.
16. Yang L, Xu L, Yan Z, Yu W, Fan Z, Lv B, *et al.* Low dose 320-row CT for left atrium and pulmonary veins imaging-the feasibility study. *Eur J Radiol* 2012; **81**: 1549-54.
17. Stárek Z, Lehar F, Jež J, Wolf J, Novák M. 3D X-ray imaging methods in support catheter ablations of cardiac arrhythmias. *Int J Cardiovasc Imaging* 2014; **30**: 1207-23.
18. Kriatselis C, Tang M, Roser M, Fleck E, Gerds-Li H. A new approach for contrast-enhanced X-ray imaging of the left atrium and pulmonary veins for atrial fibrillation ablation: rotational angiography during adenosine-induced asystole. *Europace* 2009; **11**: 35-41.
19. Tang M, Kriatselis C, Ye G, Nedios S, Roser M, Solowjowa N, *et al.* Reconstructing and registering three-dimensional rotational angiogram of left atrium during ablation of atrial fibrillation. *Pacing Clin Electrophysiol* 2009; **32**: 1407-16.
20. Nölker G, Asbach S, Gutleben KJ, Rittger H, Ritscher G, Brachmann J, *et al.* Image-integration of intraprocedural rotational angiography-based 3D reconstructions of left atrium and pulmonary veins into electroanatomical mapping: accuracy of a novel modality in atrial fibrillation ablation. *J Cardiovasc Electrophysiol* 2010; **21**: 278-83.
21. Knecht S, Wright M, Akrivakis S, Nault I, Matsuo S, Chaudhry GM, *et al.* Prospective randomized comparison between the conventional electroanatomical system and three-dimensional rotational angiography during catheter ablation for atrial fibrillation. *Heart Rhythm* 2010; **7**: 459-65.
22. Sra J, Krum D, Malloy A, Bhatia A, Cooley R, Blanck Z, *et al.* Posterior left atrial-esophageal relationship throughout the cardiac cycle. *J Interv Card Electrophysiol* 2006; **16**: 73-80.
23. Wongcharoen W, Tsao HM, Wu MH, Tai CT, Chang SL, Lin YJ, *et al.* Morphologic characteristics of the left atrial appendage, roof, and septum: implications for the ablation of atrial fibrillation. *J Cardiovasc Electrophysiol* 2006; **17**: 951-6.

24. Wielandts JY, De Buck S, Ector J, Nuyens D, Maes F, Heidbuchel H. Left ventricular four-dimensional rotational angiography with low radiation dose through interphase registration. *Europace* 2015; **17**: 152-9.
25. Prümmer M, Hornegger J, Lauritsch G, Wigström L, Girard-Hughes E, Fahrig R. Cardiac C-arm CT: a unified framework for motion estimation and dynamic CT. *IEEE Trans Med Imaging* 2009; **28**: 1836-49.
26. Lauritsch G, Boese J, Wigström L, Kemeth H, Fahrig R. Towards cardiac C-arm computed tomography. *IEEE Trans Med Imaging* 2006; **25**: 922-34.
27. Müller K, Schwemmer C, Hornegger J, Zheng Y, Wang Y, Lauritsch G, et al. Evaluation of interpolation methods for surface-based motion compensated tomographic reconstruction for cardiac angiographic C-arm data. *Med Phys* 2013; **40**: 03110.
28. Müller K, Maier AK, Schwemmer C, Lauritsch G, De Buck S, Wielandts JY, et al. Image artefact propagation in motion estimation and reconstruction in interventional cardiac C-arm CT. *Phys Med Biol* 2014; **59**: 3121-38.
29. Tan N, Liu Y, Chen JY, Zhou YL, Li X, Li LW, et al. Use of the contrast volume or grams of iodine-to-creatinine clearance ratio to predict mortality after percutaneous coronary intervention. *Am Heart J* 2013; **165**: 600-8.
30. Wielandts JY, De Buck S, Ector J, Lagerche A, Willems R, Bosmans H, et al. Three-dimensional cardiac rotational angiography: effective radiation dose and image quality implications. *Europace* 2010; **12**: 194-201.
31. The 2007 Recommendations of the International Commission on Radiological Protection. *Ann ICRP* 2007 2007; **37**: 1-332.
32. Kalender WA, Hebel R, Ebersberger J. Reduction of CT artifacts caused by metallic implants. *Radiology* 1987; **164**: 576-577.
33. Crum WR, Camara O, Hill DL. Generalized overlap measures for evaluation and validation in medical image analysis. *IEEE Trans Med Imaging* 2006; **25**: 1451-61.

34. Kautzner J, Peichl P. 3D and 4D echo-applications in EP laboratory procedures. *J Interv Card Electrophysiol* 2008; **22**: 139-44.
35. Dausch DE, Castellucci JB, Gilchrist KH, Carlson JB, Hall SD, von Ramm OT. Live volumetric imaging (LVI) intracardiac ultrasound catheter. *Cardiovasc Revasc Med* 2013; **14**: 157-9.
36. Kliger C, Cruz-Gonzalez I, Ruiz CE. The present and future of intracardiac echocardiography for guiding structural heart disease interventions. *Rev Esp Cardiol* 2012; **65**: 791-4.
37. Qin J, Liu LY, Fang Y, Zhu JM, Wu Z, Zhu KS, et al. 320-detector CT coronary angiography with prospective and retrospective electrocardiogram gating in a single heartbeat: comparison of image quality and radiation dose. *Br J Radiol*; 2012, **85**:945-51.
38. Wright M, Harks E, Deladi S, Suijver F, Barley M, van Dusschoten A, et al. Real-time lesion assessment using a novel combined ultrasound and radiofrequency ablation catheter. *Heart Rhythm* 2011; **8**: 304-12.
39. Balonov MI, Shrimpton PC. Effective dose and risks from medical x-ray procedures. *Ann ICRP* 2012 2012; **41**: 129-141.
40. Van Slambrouck K, Nuyts J. Metal artifact reduction in computed tomography using local models in an image block-iterative scheme. *Med Phys* 2012; **39**: 7080-93.
41. Kratz B, Weyers I, Buzug TM. A fully 3D approach for metal artifact reduction in computed tomography. *Med Phys* 2012; **39**: 7042-54.

Table 1:Quantitative Assessment of Image Quality.

	Original 4DRA Reconstructions (n=55)	p value	Post-Processed 4DRA Reconstructions (n=55)	p value	Original 3DRA Reconstructions (n=11)
Image Noise [GV]	447.6 ± 49.4	<0.0001	62.5 ± 21.5	<0.0001	249.4 ± 77.6
Signal Intensity LV Cavity [GV]	1549.1 ± 97.9	0.871	1552.0 ± 88.9	<0.0001	2060.0 ± 211.1
Signal Intensity LV Wall [GV]	1224.6 ± 33.5	0.669	1222.2 ± 24.1	<0.0001	1156.2 ± 65.5
Contrast [GV]	324.5 ± 96.6	0.764	329.8 ± 87.4	<0.0001	904.7 ± 200.5
Contrast-to-Noise Ratio	0.7 ± 0.2	<0.0001	5.7 ± 1.9	0.005	3.8 ± 1.0

Data are presented as mean \pm sd. GV = Gray Value.

Table 2:Projected 3D Models and Angiography Similarity Assessment.

	RAO (n=55)	LAO (n=55)	p value	MAX DIASTOLE (n=11)	SYSTOLE (n=14)	MAX SYSTOLE (n=11)	DIASTOLE (n=19)	p value
RMS CPD [mm]	2.8 ± 0.8	2.8 ± 0.7	0.690	2.7 ± 0.7	2.8 ± 0.7	2.9 ± 0.8	2.8 ± 0.7	0.523
CPD <4mm [%]	94.7 ± 6.4	95.8 ± 4.5	0.293	95.8 ± 4.9	95.9 ± 4.5	94.9 ± 7.2	94.3 ± 5.8	0.656
Dice coefficient [%]	93.8 ± 2.2	94.8 ± 1.5	0.005	94.9 ± 2.2	94.4 ± 1.4	93.6 ± 2.1	94.1 ± 2.1	0.151

Data are presented as mean±sd. CPD = closest point distance, RMS = root mean squared. Left panel: overall results in RAO and LAO. Right panel: acquired cardiac phases grouped per stage in the cardiac cycle (maximum systole, maximum diastole, systolic stage and diastolic stage).

Figure Legends.**Figure 1:**

Single phase reconstruction using 20 3DRA projections shown as a coronal (1), axial (2) and sagittal (3) slice through the LVOT (orange crosshairs) before (A) and after (B) streak artifact reduction and interphase registration-based filtering. Yellow arrows indicate catheter tips and respective artifacts prior to removal. A clear reduction of overall noise between panel A and B can be observed, allowing characterization of left atrium (LA), left ventricle (LV), anterior (a) and posterior (p) papillary muscles and aortic structures (Ao).

Figure 2:

LV cavity segmentation of diastolic (left/blue) and systolic (right/green) phase in one patient. Despite very high noise and artifact load in the original reconstructed images, the presented post-processing method allows anatomic detail to be preserved throughout the cardiac cycle: Anterior (1) and posterior papillary muscle (2), apex (3), LVOT (4), Aortic sinus (5), LV Inflow (6).

Figure 3:

Image integration of the 4D model with the fluoroscopy system shown in RAO (left panel) and LAO (right panel) for the diastolic (blue) and systolic (green) phase respectively in semi-transparent overlay with the corresponding angiography frame. Both Dynamic 3DRA and fluoroscopy were acquired during atrial pacing at 700 ms (see ECG) by means of a catheter in the right atrial appendage (1) and with iodine contrast injection in the LA through a pigtail catheter (2a) via a transseptal sheath (2b). An oesophageal temperature probe (3) is present. The marks on the ECG strip correspond to the timing of the acquired 3DRA projections, the blue and green marks to the timing of the diastolic respectively systolic phase. An accurate overlay can be seen with LV inflow (4a), LVOT/Aortic Sinus (4b) and papillary structures (4c). Slight mismatch can be observed at locations with substantial LV wall trabeculation and is inherent to segmentation by thresholding (4d).

Figure 4:

Plot showing the relationship between the estimated Effective Dose (ED), calculated using a Monte-Carlo simulation-based method, and the Dose-Area Product (DAP) reported by the 3DRA system.

Figure 5:

Cumulative processing time for generating a 5-phase 4DRA segmentation (blue), shown alongside the time needed for generating a clinical static 3DRA segmentation (black). The horizontal axis shows the different steps in chronological order: acquisition (ACQ), reconstruction based on all projection images: 67 for 3DRA, 100 for 4DRA (REC all), streak artifact reduction (SAR), separate 5-phase reconstruction of the updated projection images (REC 5ph), IPR-based filtering (IPR) and segmentation step (SEGM). White dots indicate that a particular step is not performed. Future technical refinements may further shorten this time. The extra time investment of ± 9 min for 4DRA should also be put in contrast to the time necessary for sedation or anesthesia and placement of an extra ventricular rapid pacing catheter or administration of adenosine in static 3DRA.

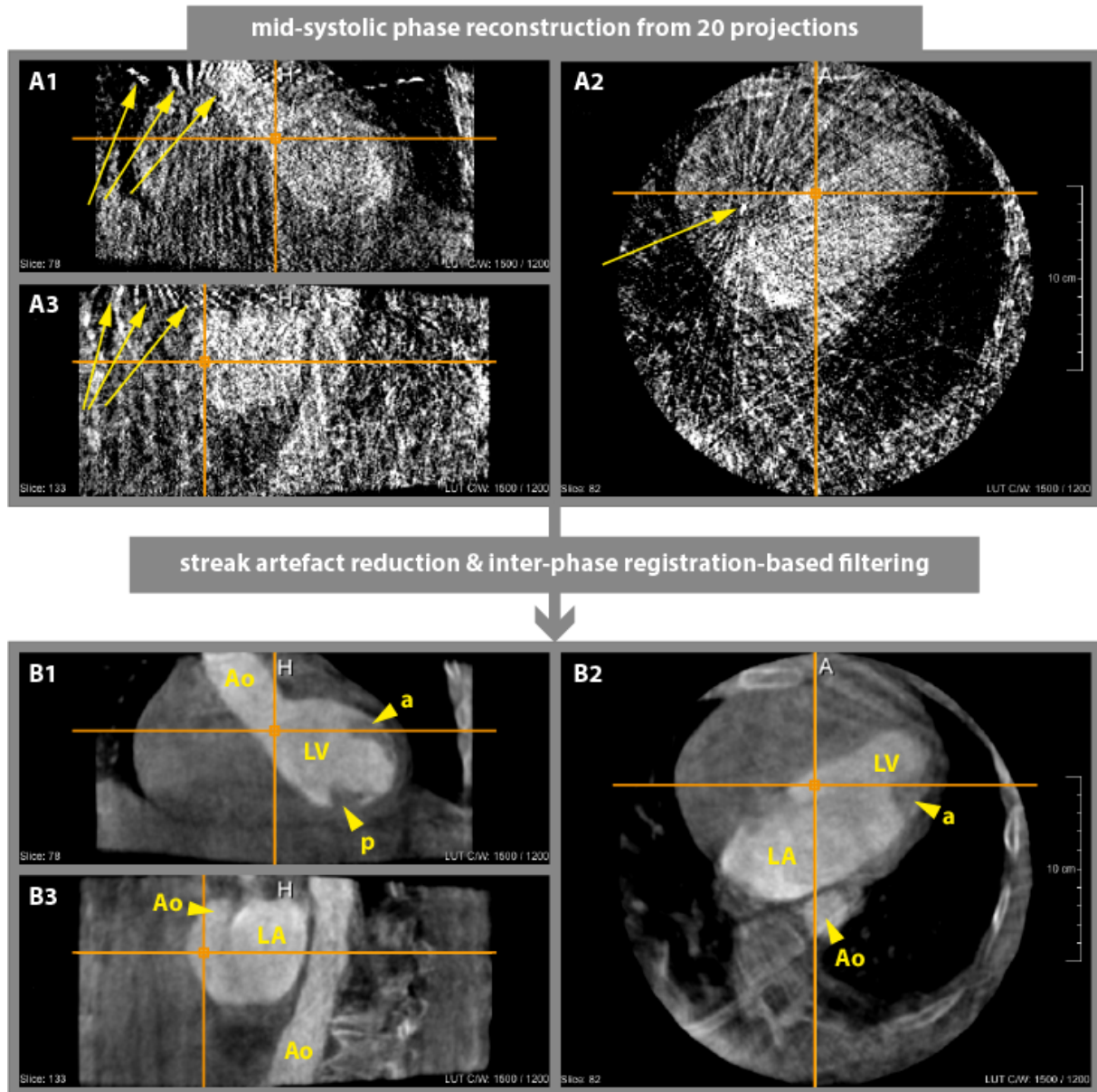
Figure 1

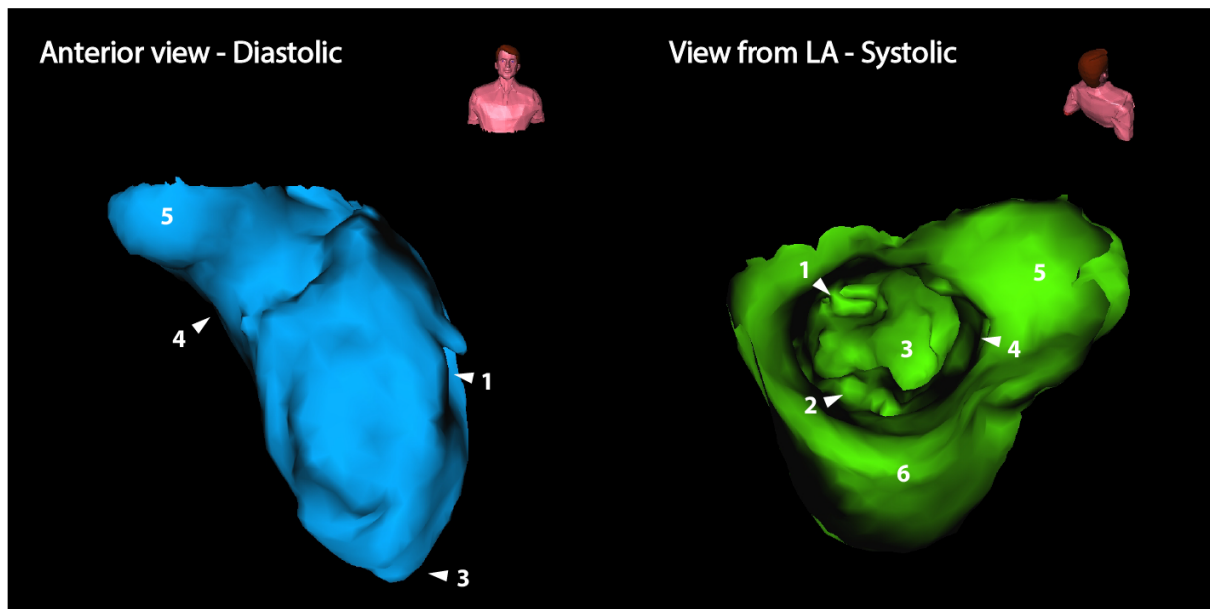
Figure 2

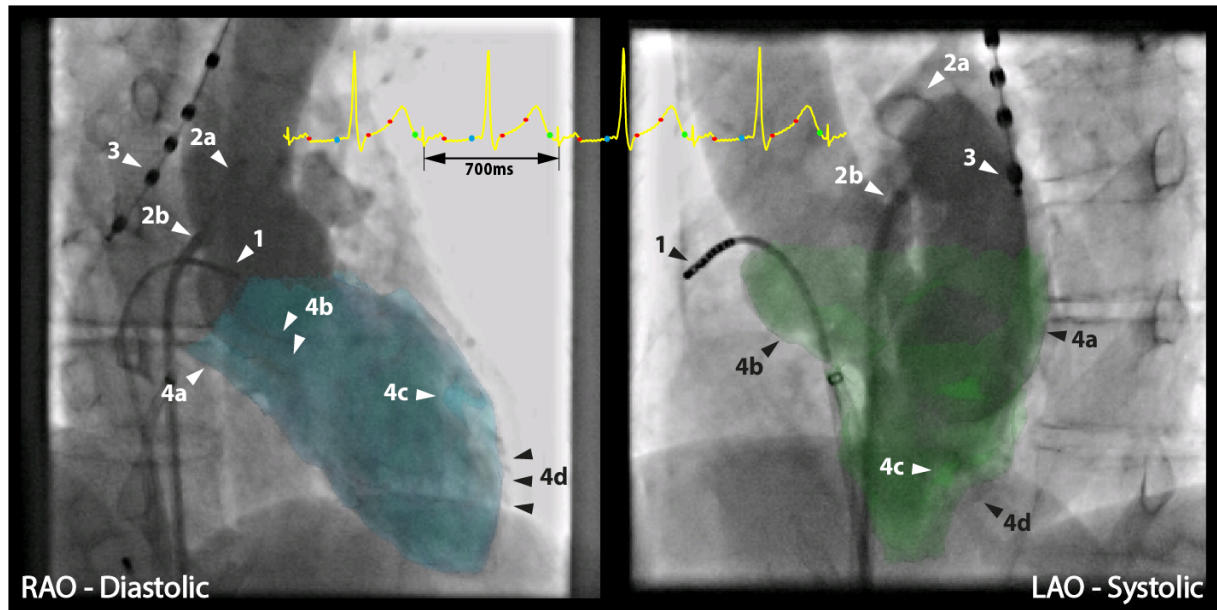
Figure 3

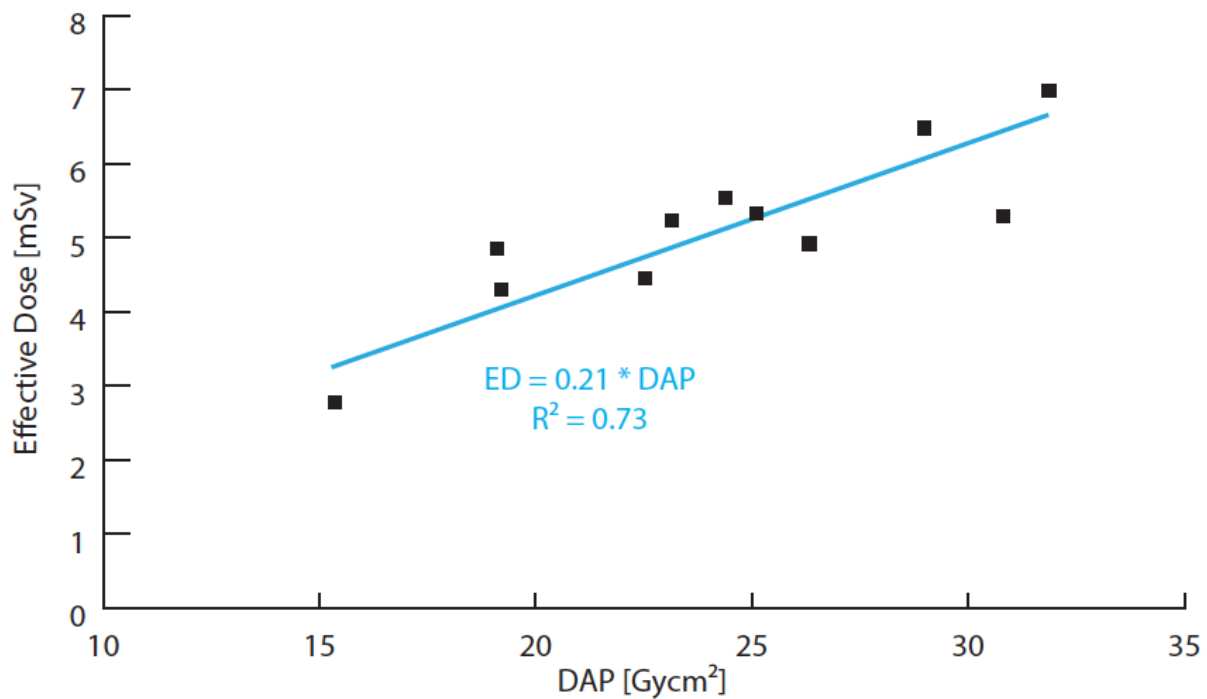
Figure 4

Figure 5